Mineralogical Magazine (2023), **87**, 611–618
doi:10.1180/mgm.2023.16

CAMBRIDGE UNIVERSITY PRESS

Article

Dongchuanite, a new phosphate mineral with a new structure, from Dongchuan copper mine, Yunnan Province, China

Guowu Li[1], Ningyue Sun[1], Hongtao Shen[2], Yuan Xue[1], Jinhua Hao[1] and Jeffrey de Fourestier[3]

[1]Science Research Institute, China University of Geosciences, 100083 Beijing, P.R. China; [2]School of Resources and Environmental Engineering, Wuhan University of Technology, 430070 Wuhan, P.R. China and [3]State Key Laboratory of Nuclear Resources and Environment, East China University of Technology, Nanchang 330013, P.R. China

Abstract

Dongchuanite, ideally $Pb_4^{VI}Zn^{IV}Zn_2(PO_4)_2(PO_4)_2(OH)_2$, is a new phosphate mineral with a new type of structure. It was found at the Dongchuan copper mine, Yunnan Province, People's Republic of China. Dongchuanite generally occurs as spherical aggregates with microscopic lamellar crystals, characterised by a turquoise–greenish blue colour. It is transparent, with a colourless streak and has a vitreous lustre without fluorescence. It is brittle with a Mohs hardness of 2–2½, and has good parallel cleavage to {011}, with insignificant parting and even fracture. According to the empirical formula and cell volume, it has a calculated density of 6.06 g/cm^3. It easily dissolves in acid without gas being emitted. The mineral is biaxial (–), calculated $n = 1.90$ and maximum birefringence: $\delta = 0.010$ and 2V=70°. Dispersion of the optical axes $r < v$ is very weak. The mineral is pale blue to light blue and very weakly pleochroic in transmitted light. Dongchuanite crystallises in the triclinic space group $P\bar{1}$, with unit-cell parameters $a = 4.7620(10)$ Å, $b = 8.5070(20)$ Å, $c = 10.3641(19)$ Å, $\alpha = 97.110(17)°$, $\beta = 101.465(17)°$, $\gamma = 92.273(18)°$, $V = 407.44(15)$ Å^3 and $Z = 1$. The eight strongest reflections in the powder X-ray diffraction pattern [d_{obs}, Å (I/I_0) (hkl)] are: 3.442 (100) ($\bar{1}12$), 3.035 (50) (120), 4.652 (45) (100), 2.923 (40) ($\bar{1}\bar{1}3$), 2.384 (35) ($\bar{2}01$), 3.130 (30) ($\bar{1}21$), 2.811 (30) (030) and 2.316 (18) (032). The crystal structure (solved and refined from single-crystal X-ray diffraction data, $R_1 = 0.07$) is a new layered structure consisting of corner-sharing tetrahedrons and octahedrons, where [PO_4] tetrahedra and [ZnO_4] tetrahedra share corners to form a double chain, and the another [PO_4] tetrahedra is connected by corner-sharing with a [$ZnO_4(OH)_2$] octahedra to form a tetrahedral–octahedral chain, extending along the a-axis direction. The two types of chains are connected by corner-sharing between [ZnO_4] and [PO_4] tetrahedra forming a wrinkled layer parallel to (011). The Pb atoms occupy two independent sites between the wrinkled layers, both of which have typical lopsided coordination of Pb^{2+} with stereoactive $6s^2$ lone-pair electrons.

Keywords: dongchuanite, new mineral species, phosphate, supergene mineral, crystal structure, Dongchuan copper mine

(Received 30 May 2022; accepted 27 February 2023; Accepted Manuscript published online: 24 May 2023; Associate Editor: Irina O Galuskina)

Introduction

Located in the northeast of Yunnan Province, 160 km north of Kunming City, the Dongchuan copper mine, an important Chinese copper ore deposit, has been made famous for copper production and the supply of raw materials for minting coins for ancient dynasties. Owing to its unique geological conditions and deposit characteristics, the Dongchuan copper mine has become well known within China for its rare layered super-large sediment-hosted stratiform copper deposits (Leach and Song, 2019). Our recent findings have revealed several new supergene arsenate–phosphate minerals in the region including dongchuanite (IMA2021-058, Li *et al.*, 2021), cuprodongchuanite (IMA2021-065, Sun *et al.*, 2021), zheshengite (IMA2022-011, Li *et al.*, 2022) and cuprozheshengite (IMA2021-095a, Sun *et al.*, 2022). All have the same general crystal chemical formula and crystal structure type and have no natural or synthetic analogues. The first of these minerals is dongchuanite.

The new mineral species and its name (symbol Dc) have been approved by the Commission on New Minerals, Nomenclature and Classification (CNMNC) of the International Mineralogical Association (IMA2021-058, Li *et al.*, 2021). The holotype specimen of dongchuanite is under catalogue number No. M26148 at the Geological Museum of China (Xisi Yangrou Hutong No. 15, Xicheng District, Beijing), P.R. China.

Occurrence and associated minerals

Dongchuanite was found at Sanguozhuang Village, Tangdan Town, Dongchuan District, Kunming City, Yunnan Province, P.R. China (26°8'14"N, 102°59'36"E), and located in the east of the Dongchuan copper ore field.

The Dongchuan copper ore field is composed of multiple spatially independent deposits with the same origin. The proven

Corresponding author: Guowu Li; Email: liguowu@cugb.edu.cn
Cite this article: Li G., Sun N., Shen H., Xue Y., Hao J. and de Fourestier J. (2023) Dongchuanite, a new phosphate mineral with a new structure, from Dongchuan copper mine, Yunnan Province, China. *Mineralogical Magazine* **87**, 611–618. https://doi.org/10.1180/mgm.2023.16

copper deposits are Sikeshu, Yikeshu, Yinming, Luoxue, Sijiangjun, Baixina, Lanniping, Tangdan and Xintang (Zhang *et al.*, 2021). The surrounding ore-bearing rock is from the Mesoproterozoic Dongchuan Group and a small number of Shinian Doushantuo Formation strata. There are different views as to the origin of the ore deposit. However, it is generally believed that it was formed by sedimentation–hydrothermal transformation (Zeng *et al.*, 2021; He, 1996). There are a wide variety of mineral species in the deposits, with more than 20 species of polymetallic sulfide minerals and more than 30 supergene minerals identified so far. Dongchuanite was found in an abandoned mine shaft, which is ~1.7 km northwest of Sanguozhuang Village, where the altitude is over 3000 metres. This mine is located on the southern limb of the Huangcaoling syncline. Dongchuanite occurs on a sandstone fracture around Cu-sulfide ore veins, and are clearly of supergene origin. The new minerals may have been formed by the weathering of copper, lead and zinc sulfides under the action of surface water. Associated minerals are quartz, theisite, veszelyite, kipushite, tangdanite, tyrolite, arsenoveszelyite, bayldonite, cuprodongchuanite and hemimorphite.

Morphology and physical properties

Dongchuanite is composed of spherical aggregates of microscopic lamellar crystals. The size of the spherical aggregates range from 0.5 to 1 mm (Fig. 1). The thickness of single lamellar crystals ranges from 5 to 20 μm (Fig. 2). The crystal habit of the radial aggregates of tiny lamellar crystals is parallel to {010} with chisel-like terminations of {011}; the forms are {100}, {010}, {011} and {0$\bar{1}$1} (Fig. 3) with unobserved twinning. It is characteristically turquoise–greenish blue and transparent, with a colourless streak, a vitreous lustre and is non-fluorescent. Dongchuanite is brittle with a Mohs hardness of 2–2½, and a micro-hardness (VHN load in 10 g) mean of 91.3 and a range of 85.7–96.4 (kg/mm^2). It has good cleavage parallel to {011}, parting was not observed and the fracture is even. The density could not be measured directly because of the small size of individual crystals. Based on the empirical formula and cell volume, the calculated density is 6.06 g/cm^3. Dongchuanite is dissolved easily in dilute hydrochloric acid and without gas evolution. The mineral is biaxial (–). The anisotropic refractive index was not measured as that of the mineral is higher than that of the highest refractive oil. The calculated Gladstone–Dale relation is $n = 1.90$ by $N = K_d + 1$ (Mandarino, 1981). The maximum birefringence: $\delta = 0.010$ (estimation from the highest interference colour from a section of 30 μm thickness) and $2V_{meas.} = 70°$. Dispersion of the optical axes $r < v$ is very weak. Optical axes could not be determined due to the form of the microcrystal aggregates. In transmitted light, the mineral is pale blue to light blue and is very weakly pleochroic.

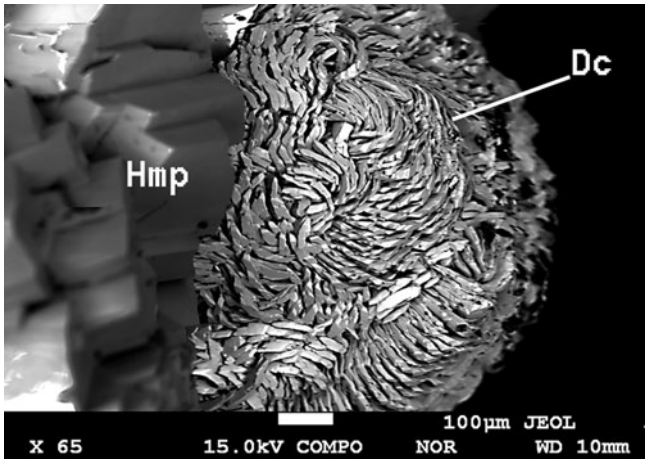

Figure 2. Scanning electron microscopy image of the crystal for dongchuanite (#M26148, holotype DC-1) on hemimorphite (Hmp).

Chemical composition

The chemical composition of dongchuanite was determined using a JXA-8230 electron microprobe (wavelength dispersive mode) with settings of: acceleration voltage = 15 kV, beam current =

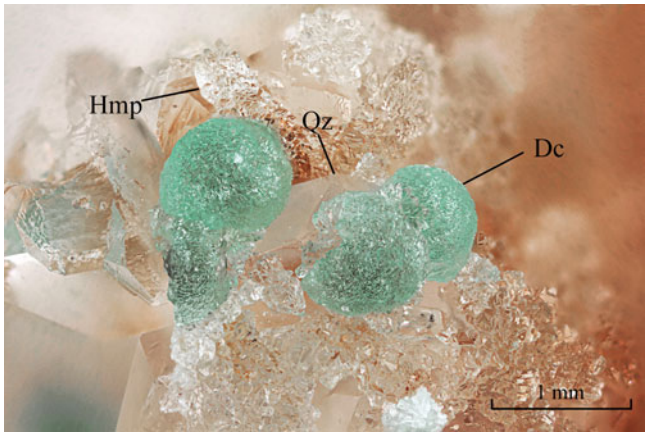

Figure 1. Spherical radial aggregates of dongchuanite (Dc) associated with hemimorphite (Hmp) and quartz (Qz) (#M26148, holotype DC-1).

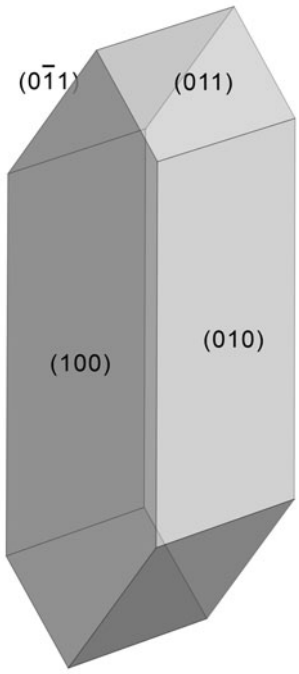

Figure 3. The ideal lamellar crystal shape for for dongchuanite.

https://doi.org/10.1180/mgm.2023.16 Published online by Cambridge University Press

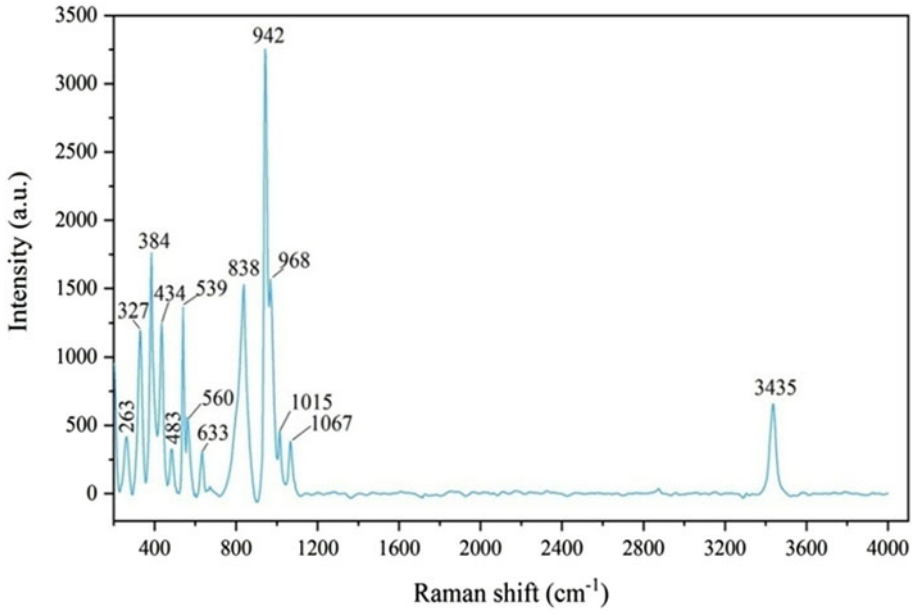

Figure 4. Raman spectrum of dongchuanite.

5 nA, beam diameter = 5 μm and number of analyses = 8 points on one grain. The average component of the dongchuanite aggregate for the following structure refinement is acceptable. We did not collect a sufficient amount of material for direct determination of H_2O, so it was confirmed by Raman spectrum analysis, as shown in Fig. 4. Crystal structure refinement and bond-valence sum analysis showed that O9 is the only oxygen in the form of OH^-. Subsequently, we calculated the H_2O amount based on the O9 site as fully occupied by OH^-. The chemical composition and compositional ranges of dongchuanite are shown in Table 1. The empirical formula (based on O = 18 atoms per formula unit) is $(Pb_{3.92}Cd_{0.02})_{\Sigma 3.94}(Zn_{0.69}Cu_{0.45})_{\Sigma 1.14}Zn_2[(P_{0.67}As_{0.29}S_{0.01})_{\Sigma 0.97}O_4]_2(PO_4)_2(OH)_2$. The simplified formula is: $Pb_4(Zn,Cu)Zn_2[(P,As)O_4]_2(PO_4)_2(OH)_2$. The ideal formula is: $Pb_4^{VI}Zn^{IV}Zn_2(PO_4)_2(PO_4)_2(OH)_2$, which requires PbO 62.05, ZnO 16.97, P_2O_5 19.73, H_2O 1.25, total 100 wt.%.

Raman spectroscopy

The Raman spectrum of dongchuanite was obtained by using a Horiba Via-Reflex, in a reflection mode with a laser excitation wavelength of 532 nm and 600 gr/mm. The spectrum in the 200–4000 cm^{-1} region was obtained using the collection time of 20 s and 2 scans with a resolution of 4 cm^{-1}.

The Raman spectrum pattern is shown in Fig. 4. Bands in the range 600 to 200 cm^{-1} comprise partially overlapped bands assigned to the υ_4 (and υ_2) vibrations of the PO_4 (AsO_4) tetrahedrons, vibrations of the ZnO_4 tetrahedra, Zn-, Pb-centred polyhedrons and lattice modes. The bands at 560, 539 and 483 cm^{-1}can be assigned to υ_4(O–P–O). Bands at 384 and 327 cm^{-1} corresponded to υ_2(O–P–O) (Frost *et al.*, 2002). The band at 434 cm^{-1} probably corresponds to ZnO_4 tetrahedra vibration, the symmetric stretching mode of the ZnO_4 tetrahedron (Hawthorne *et al.*, 2012). The band at 263 cm^{-1} can be assigned to M(Pb,Zn,Cu)–O vibration (Frost *et al.*, 2002; Ciesielczuk *et al.*, 2016).

Bands in the range of 1100–600 cm^{-1} are ascribed to the stretching vibrations of $(PO_4)^{3-}$ and $(AsO_4)^{3-}$ (Farmer, 1974). Two groups of splitting peaks related to $(PO_4)^{3-}$ are confirmed to be υ_3 (1067 and 1015 cm^{-1}) and υ_1 (968 and 942 cm^{-1}) modes respectively. The existence of υ-splitting peaks indicates two different positions of the phosphate ion. The peak at 838 cm^{-1} is assigned to the υ_3 mode of $(AsO_4)^{3-}$, and the weak peak at 633 cm^{-1} ascribed to υ_2 $(PO_4)^{3-}$ vibration.

Sharp stretching vibrations corresponding to hydroxyl ions are found at 3435 cm^{-1}. However there are no H_2O-molecule bending modes in the 1600–1700 cm^{-1} region, which proves that OH^- is the only water present (Grey *et al.*, 2017).

Table 1. Chemical data (in wt.%) for dongchuanite.

Constituent	Mean	Range	S.D. (σ)	Reference material
BaO	0.05	0.00–0.16	0.06	$BaSO_4$
CdO	0.21	0.15–0.29	0.05	Cd
As_2O_5	4.62	3.92–5.2	0.52	FeAsS
SiO_2	0.03	0.00–0.08	0.03	SiO_2
ZnO	14.91	14.35–15.44	0.31	$(ZnMn)_2SiO_4$
CuO	2.45	2.13–2.72	0.20	$CuFeS_2$
FeO	0.02	0.00–0.06	0.02	Fe_2O_3
V_2O_3	0.01	0.00–0.05	0.02	V
PbO	59.59	58.55–60.62	0.67	$PbCrO_4$
SO_3	0.05	0.00–0.09	0.03	$SrSO_4$
P_2O_5	16.19	15.46–16.93	0.49	$Ca_5(PO_4)_3F$
H_2O*	1.23			
Total	99.37	98.27–100.67	0.74	

*Calculated from crystal structure refinement.
S.D. – standard deviation.

Powder X-ray diffraction

The powder X-ray diffraction pattern for dongchuanite was recorded using a Rigaku-Oxford diffraction XtaLAB PRO-007HF single-crystal diffractometer equipped with a hybrid pixel array plane detector, with the method of rotating a crystal using a 20 μm grain. A Gandolfi-like motion on the φ and ω axes was used to randomise the sample. The detector was set to a distance of 114 mm, and with detector 2θ-axis 0° and ±35° images superposition, to improve the resolution of powder diffraction lines. The observed *d* values and intensities were derived by profile fitting using *Search-Match* software (Siegrist, 1997).

https://doi.org/10.1180/mgm.2023.16 Published online by Cambridge University Press

Table 2. Powder X-ray diffraction data (*d* in Å) for dongchuanite.*

I_{obs}	I_{calc}	d_{obs}	d_{calc}	*h*	*k*	*l*	I_{obs}	I_{calc}	d_{obs}	d_{calc}	*h*	*k*	*l*	I_{obs}	I_{calc}	d_{obs}	d_{calc}	*h*	*k*	*l*
2	2	8.3605	8.4197	0	$\bar{1}$	0	1	7	2.1644	2.1682	2	0	1	3	4	1.2724	1.2785	0	$\bar{5}$	6
3	8	6.9780	6.9382	0	$\bar{1}$	1	4	8	2.1200	2.1186	0	$\bar{4}$	1	5	2	1.2393	1.2395	$\bar{1}$	3	7
10	31	6.0947	6.0689	0	1	1	12	11	2.0237	2.0236	1	2	3	4	2	1.2092	1.2100	$\bar{1}$	$\bar{6}$	5
1	8	5.0500	5.0364	0	0	2	5	12	1.9629	1.9619	2	0	2	4	2	1.1836	1.1831	$\bar{3}$	5	1
45	**53**	**4.6519**	**4.5921**	**$\bar{1}$**	**0**	**1**	8	9	1.9027	1.9030	0	$\bar{4}$	3	3	2	1.1603	1.1602	$\bar{2}$	6	3
13	21	4.2330	4.2098	0	2	0	**17**	**17**	**1.8582**	**1.8647**	**2**	**1**	**2**	1	2	1.1335	1.1341	$\bar{3}$	4	5
14	4	4.0808	4.0856	0	1	2	9	7	1.7810	1.7938	$\bar{1}$	$\bar{4}$	3	1	1	1.1168	1.1158	0	5	6
5	15	3.9279	3.9237	1	0	1	6	12	1.7433	1.7452	1	2	4	<1	1	1.1103	1.1101	$\bar{4}$	2	4
3	8	3.7159	3.7099	0	2	1	6	12	1.7166	1.7176	$\bar{1}$	$\bar{3}$	5	1	1	1.0923	1.0948	0	3	8
100	**100**	**3.4419**	**3.4288**	$\bar{1}$	**1**	**2**	10	2	1.6804	1.6812	1	$\bar{2}$.	5	1	1	1.0712	1.0712	$\bar{4}$	2	5
6	45	3.2782	3.2748	0	$\bar{1}$.	3	8	9	1.6419	1.6415	2	3	1	<1	2	1.0638	1.0625	$\bar{4}$	0	6
30	**65**	**3.1302**	**3.1170**	**$\bar{1}$**	**2**	**1**	3	2	1.5809	1.5801	$\bar{3}$	0	1	3	2	1.0479	1.0487	0	$\bar{4}$	9
50	**54**	**3.0347**	**3.0519**	**1**	**$\bar{1}$**	**2**	4	6	1.5482	1.5481	1	5	0	1	2	1.0227	1.0215	0	$\bar{8}$	4
40	**66**	**2.9231**	**2.9244**	**$\bar{1}$**	**$\bar{1}$**	**3**	7	4	1.5050	1.4989	$\bar{2}$	$\bar{3}$	5	1	2	1.0081	1.0022	$\bar{2}$	$\bar{1}$	10
30	**44**	**2.8106**	**2.8066**	**0**	**3**	**0**	4	2	1.4924	1.4915	0	2	6	1	1	0.9960	0.9960	$\bar{3}$	3	8
<1	1	2.7054	2.7211	1	2	1	4	7	1.4562	1.4548	$\bar{3}$	$\bar{2}$	1	2	1	0.9771	0.9846	3	$\bar{7}$	0
9	13	2.6130	2.6060	0	$\bar{3}$	2	3	2	1.4435	1.4427	$\bar{3}$	$\bar{2}$	3	1	1	0.9605	0.9604	4	$\bar{3}$	4
6	21	2.4934	2.4828	1	$\bar{1}$	3	6	5	4029	1.4083	$\bar{3}$	3	1	2	1	0.9443	0.9435	$\bar{1}$	$\bar{6}$	9
35	**59**	**2.3843**	**2.3725**	**$\bar{2}$**	**0**	**1**	4	1	3604	1.3605	2	4	2	1	1	0.9371	0.9371	0	4	9
18	4	2.3165	2.3127	0	$\bar{3}$	3	2	3	1.3494	1.3414	1	2	6							
6	6	2.2195	2.2202	$\bar{2}$	1	2	6	4	1.3146	1.3119	$\bar{1}$	$\bar{6}$	3							

*The strongest lines are given in bold.

Table 2 shows the powder X-ray diffraction data (for 1.2 kW micro focus rotating anode X-ray source, Mo*K*α, $\lambda = 0.71073$ Å; 50 kV/24 mA), along with the indexing and calculated intensities from the crystal structure. Unit-cell parameters refined from the powder data using *CheckCell* are: $a = 7515(1)$ Å, $b = 8.5064(2)$ Å, $c = 10.3710(2)$ Å, $\alpha = 97.090(2)°$, $\beta = 101.410(2)°$, $\gamma = 92.580(2)°$ and $V = 406.7(3)$ Å^3, which are in good agreement with those obtained from the single-crystal study (Table 2).

Single-crystal X-ray data collection and structure refinement

The single crystal X-ray diffraction data for dongchuanite were collected by using a Rigaku-Oxford diffraction XtaLAB PRO-007HF single-crystal diffractometer equipped with a rotating anode micro-focus X-ray source (1.2 kW Mo*K*α and λ = 0.71073 Å) and a hybrid pixel array detector. Similar results were obtained from two single-crystal fragments. The reflections obtained were from one single crystal fragment of excellent quality 0.02 × 0.01 × 0.01 mm in size, with $-6 < h < 6$, $-11 < k < 9$, $-13 < l < 14$ with fair $R_{int} = 0.0709$. Intensity data was corrected for Lorentz polarisation and multi-scan absorption. The space group was obtained by conducting the system extinction statistics and was found to be $P\bar{1}$. The crystal structure determination and refinement were performed using *OLEX2-1.3* (Dolomanov *et al.*, 2010) with *SHELXT* (Sheldrick, 2015). The crystal structure was solved by direct methods, which found all of the heavy atoms and part of the O atoms. According to differential-Fourier transform calculations, all O atoms were found.

The structure was refined to $R_1 = 0.07$ on the basis of 1360 independent reflections with $I > 2\sigma(I)$. The crystallographic characteristics, the experimental parameters of data collection and structure refinement are summarised in Table 3. Atom coordinates, site occupancies and geometric parameters are listed in Tables 4, 5 and 6. The crystallographic information file has been deposited with the Principal Editor of *Mineralogical Magazine* and is available as Supplementary material (see below).

Table 3. Crystal information and details of X-ray data collection and refinement.

Crystal data	
Structural formula	$Pb_4(Zn,Cu)Zn_2[(P,As)O_4]_2(PO_4)_2(OH)_2$
Crystal dimensions (mm)	0.02 × 0.01 × 0.01
Crystal system, space group	$P\bar{1}$(#2), triclinic
Temperature (K)	296(2)
a, *b*, *c* (Å)	4.7620(10), 8.5070(20), 10.3641(19)
α, β, γ (°)	97.110(17), 101.465(17), 92.273(18)
V (Å^3)	407.44(15)
Z	1
Absorption μ (mm^{-1})	47.315
$D_{calc.}$ (g cm^{-3})	6.06
Data collection	
Crystal description	turquoise–greenish blue, brittle
Diffractometer	Rigaku-Oxford diffraction XtaLAB PRO-007HF
Radiation type, wavelength (Å)	Mo*K*α (0.71073)
Scanning mode	ω scan, δω = 0.5°
max θ (°)	29.319
Absorption correction	multi-scan absorption
T_{min}, T_{max}	0.576, 0.627
No. of measured, independent and observed [$I > 2\sigma(I)$] reflections	4234, 1896, 1360
R_{int}	0.0709
Indices range of *h*, *k*, *l*	$-6 \le h \le 6$, $-11 \le k \le 9$, $-13 \le l \le 14$
Refinement	
No. of refined parameters	135
Residuals *R* [$I >= 2\sigma(I)$]	0.07
wR_2 ([$I >= 2\sigma(I)$])	0.143
Goodness of fit, S	1.059
Weighting scheme	$w = 1/[\sigma^2(Fo^2) + (0.0739P)^2]$
where $P = [max(F_o)^2 + 2(F_c)^2]/3$	
$\Delta\rho_{max}$, $\Delta\rho_{min}$ (e^- Å^{-3})	5.74/–2.99

Site-population assignment for dongchuanite

The Pb cations occupy two independent 8-coordinate sites in the interlayer region. Although the difference-Fourier map displays several ~5e^- residuals at ~1 Å around these (heavy) Pb atoms,

https://doi.org/10.1180/mgm.2023.16 Published online by Cambridge University Press

Table 4. Atomic coordinates and site occupancies* for dongchuanite.

Atom	Wyk.	*x/a*	*y/b*	*z/c*	U_{eq}
Pb1	2i	0.1497(2)	0.48048(11)	0.32941(9)	0.0221(3)
Pb2	2i	−0.1109(2)	0.10508(12)	−0.16008(10)	0.0280(3)
Zn1*	1c	0	½	0	0.0209(9)
Zn2	2i	0.6689(6)	0.1280(3)	0.3826(3)	0.0203(6)
P1*	2i	0.4891(8)	0.2494(5)	0.0886(4)	0.0181(14)
P2	2i	1.2414(12)	0.2207(7)	0.5660(6)	0.0143(12)
O1	2i	1.317(4)	0.103(2)	0.6637(16)	0.026(4)
O2	2i	1.382(4)	0.388(2)	0.6212(17)	0.032(5)
O3	2i	1.293(4)	0.162(2)	0.4251(16)	0.031(4)
O4	2i	0.908(4)	0.241(2)	0.5435(17)	0.031(4)
O5	2i	0.696(4)	0.212(2)	0.2193(18)	0.035(5)
O6	2i	0.675(3)	0.281(2)	−0.0190(16)	0.021(4)
O7	2i	0.263(4)	0.107(2)	0.0329(17)	0.028(4)
O8	2i	0.324(4)	0.403(2)	0.1253(16)	0.029(4)
O9(OH)	2i	−0.078(3)	0.6180(19)	0.1640(16)	0.022(4)

*Occupancies for Zn1 = 0.55Zn + 0.45Cu and for P1 = 0.64(2)P + 0.364(19)As.
Wyk. = Wyckoff position.

Table 5. Anisotropic displacement parameters (in Å^2) for dongchuanite.

Atom	U^{11}	U^{22}	U^{33}	U^{23}	U^{13}	U^{12}
Pb1	0.0193(5)	0.0262(5)	0.0216(5)	0.0030(4)	0.0056(4)	0.0052(4)
Pb2	0.0235(5)	0.0300(6)	0.0293(6)	0.0000(4)	0.0042(4)	0.0047(4)
Zn1	0.020(2)	0.029(2)	0.0138(18)	0.0005(17)	0.0038(16)	0.0104(17)
Zn2	0.0172(14)	0.0276(16)	0.0175(13)	0.0021(12)	0.0063(11)	0.0062(11)
P1	0.015(2)	0.025(2)	0.016(2)	0.0028(17)	0.0046(15)	0.0079(16)
P2	0.008(3)	0.021(3)	0.015(3)	0.000(2)	0.006(2)	0.006(2)
O1	0.024(9)	0.027(10)	0.025(9)	0.008(8)	−0.005(7)	0.013(8)
O2	0.018(9)	0.048(12)	0.028(9)	−0.010(9)	0.007(8)	0.008(8)
O3	0.018(9)	0.049(12)	0.025(9)	−0.009(9)	0.007(8)	0.009(8)
O4	0.021(7)	0.033(8)	0.035(8)	−0.014(6)	0.005(6)	0.011(6)
O5	0.033(11)	0.043(12)	0.030(10)	0.012(9)	0.004(8)	0.002(9)
O6	0.013(6)	0.026(7)	0.027(7)	0.001(6)	0.008(6)	0.008(6)
O7	0.019(9)	0.044(11)	0.029(9)	0.008(8)	0.013(7)	0.023(8)
O8	0.023(10)	0.039(11)	0.022(8)	−0.007(8)	0.005(7)	0.007(8)
O9(OH)	0.022(9)	0.021(9)	0.025(9)	−0.006(7)	0.010(7)	0.011(7)

Table 6. Selected interatomic distances (Å) for dongchuanite.

Pb1–O2^{i}	2.385 (17)	Pb2–O1^{iv}	2.994 (17)
Pb1–O2^{ii}	3.210 (19)	Pb2–O1^{v}	2.961 (16)
Pb1–O2^{iii}	2.917 (17)	Pb2–O3^{vi}	3.289 (16)
Pb1–O3^{ii}	3.050 (20)	Pb2–O4^{iv}	3.429 (19)
Pb1–O4^{iii}	2.616 (17)	Pb2–O6^{ii}	2.364 (15)
Pb1–O5^{ii}	3.030 (18)	Pb2–O7	2.397 (17)
Pb1–O8	2.449 (16)	Pb2–O7^{vii}	2.526 (18)
Pb1–O9	2.312 (18)	Pb2–O9^{viii}	2.496 (16)
<Pb1–O>	2.746	<Pb2–O>	2.807
Zn1–O6^{ii}	2.339 (16)	Zn2–O1^{x}	1.970 (17)
Zn1–O6^{ix}	2.339 (16)	Zn2–O3^{ii}	1.951 (17)
Zn1–O8	2.078 (18)	Zn2–O4	1.939 (17)
Zn1–O8^{viii}	2.078 (18)	Zn2–O5	1.940 (19)
Zn1–O9^{viii}	1.974 (15)	<Zn2–O>	1.950
Zn1–O9	1.974 (15)		
<Zn1–O>	2.130		
P1–O5	1.586 (19)	P2–O1	1.514 (18)
P1–O6	1.595 (16)	P2–O2	1.543 (19)
P1–O7	1.561 (19)	P2–O3	1.553 (17)
P1–O8	1.596 (18)	P2–O4	1.580 (18)
<P1–O>	1.585	<P2–O>	1.548

Symmetry codes: (i) −*x*+2, −*y*+1, −*z*+1; (ii) *x*−1, *y*, *z*; (iii) −*x*+1, −*y*+1, −*z*+1; (iv) *x*−1, *y*, *z*−1; (v) *x*−2, *y*, *z*−1; (vi) −*x*+1, −*y*, −*z*; (vii) −*x*, −*y*, −*z*; (viii) −*x*, −*y*+1, −*z*; (ix) −*x*+1, −*y*+1, −*z*; (x) −*x*+2, −*y*, −*z*+1; (xi) *x*+1, *y*, *z*; (xii) *x*+2, *y*, *z*+1; (xiii) *x*+1, *y*, *z*+1.

which might suggest some slight disorder, they are probably simply 'ripples' resulting from series termination effects due to the average quality of the data.

Zinc has two different crystal chemical locations in dongchuanite. Zn1 (Wyckoff position 1*c*) and Zn2 (Wyckoff 2*i*). Zn1 (Wyckoff 1*c*) has [6]-coordinates (^{VI}Zn) with O and OH forming $[Zn1O_4(OH)_2]$ octahedra, whose average bond length is 2.126 Å. The substantial Cu content of the octahedral Zn1 site, as indicated by the empirical formula based on the electron microprobe analysis, was clearly supported by the significant Jahn-Teller distortion observed (see Table 6). The average bond valences involved in linkage to Zn1 cation is 0.33. Zn2 (Wyckoff 2*i*) has [4]-coordinates (^{IV}Zn) with O forming $[ZnO_4]$ tetrahedral coordination and is fully occupied by Zn. The average bond length of Zn is 1.950 Å, and the average bond valences involved in linkage to the Zn2 cation is 0.50.

Phosphorus also has two crystal chemical locations. $[P1O_4]$ tetrahedra share corners with $[Zn2O_4]$ tetrahedra and two $[Zn1O_4(OH)_2]$ octahedra. $[P2O_4]$ tetrahedra share corners with three $[Zn2O_4]$ tetrahedra. The results of the free refinement of these two positions using P show that the occupancy of P2 is 1.06P, whereas the occupancy of P1 is 1.51P, which indicates that isomorphic substitution mainly occurs at the P1 site with heavier atoms. The final free refined occupancy of the P1 site is 0.65P + 0.35As. The average bond length of P1–O (1.581 Å) is higher than P2–O (1.539 Å). Raman spectra shows splitting peaks of $(PO_4)^{3-}$ indicating two different crystal chemical environments. P tends to occupy the crystal chemical position of the P2 site, while As tends to be predominantly at the P1 site. The results are close to the chemical composition and gave reasonable bond-valence sums (Table 7).

Although the coordinates of H are not refined in the crystal structure (due to interference of the heavy atom Pb), the Raman spectrum (Fig. 4) and bond-valence sums (Table 7) confirm that H is attached to O9 as OH^-.

Crystal structure description

Dongchuanite has a chain-layer structure, composed of a tetrahedral double chain and a tetrahedral–octahedral chain in a unit layer (Fig. 5). The tetrahedral double chain is formed by the connection of $[PO_4]$ tetrahedra and $[ZnO_4]$ tetrahedra along the [100] direction (Fig. 5b). Each tetrahedron is 3-connected with other tetrahedra in the chain. The P–O mean bond-length is 1.539 Å in the $[PO_4]$ tetrahedra, and the Zn–O mean bond length is 1.950 Å in the $[ZnO_4]$ tetrahedra. The tetrahedral–octahedral chain is formed by the $[PO_4]$ tetrahedra that share corners with $[ZnO_4(OH)_2]$ octahedra, along the [100] direction. The alternating $[ZnO_4(OH)_2]$ octahedra and pairs of corner-connected $[PO_4]$ tetrahedra are shown in Fig. 5a. The hydroxyl group is located on both sides of the centre of the Zn cation. In this chain, both the P–O and Zn–O bonds have longer distances than those bonds in the tetrahedral double chain, with an average P–O distance of 1.581 Å and a Zn–O distance of 2.126 Å. The same type of chains are present in drugmanite where PO_4 tetrahedra share corners with $(Fe,Al)O_6$ octahedra (King and Sengier-Roberts, 1988). Along the [100] direction, the tetrahedra $[ZnO_4]$–$[PO_4]$–$[ZnO_4]$ length matches the $[PO_4]$–$[ZnO_4(OH)_2]$–$[PO_4]$ length exactly, so that the two types of chains can be connected by corner-sharing between $[ZnO_4]$ and $[PO_4]$ tetrahedra, as illustrated in Fig. 6, to form wrinkled layers parallel to (011) (Fig. 7).

https://doi.org/10.1180/mgm.2023.16 Published online by Cambridge University Press

Table 7. Bond-valence sum for dongchuanite.

	Pb1	Pb2	Zn1	Zn2	P1	P2	O sum
O1		0.12+0.13 $^{\downarrow\rightarrow}$		0.47 $^{\downarrow\rightarrow}$		1.32 $^{\downarrow\rightarrow}$	2.04
O2	0.42+0.14+0.08 $^{\downarrow\rightarrow}$					1.23 $^{\downarrow\rightarrow}$	1.87
O3	0.11 $^{\downarrow\rightarrow}$	0.07 $^{\downarrow\rightarrow}$		0.49 $^{\downarrow\rightarrow}$		1.29 $^{\downarrow\rightarrow}$	1.86
O4	0.26 $^{\downarrow\rightarrow}$	0.05 $^{\downarrow\rightarrow}$		0.51$^{\downarrow\rightarrow}$		1.12 $^{\downarrow\rightarrow}$	1.94
O5	0.11 $^{\downarrow\rightarrow}$			0.51 $^{\downarrow\rightarrow}$	1.29 $^{\downarrow\rightarrow}$		1.91
O6		0.44 $^{\downarrow\rightarrow}$	0.17 $^{\times2\downarrow\rightarrow}$		1.26 $^{\downarrow\rightarrow}$		2.04
O7		0.41+0.32 $^{\downarrow\rightarrow}$			1.38 $^{\downarrow\rightarrow}$		2.11
O8	0.37 $^{\downarrow\rightarrow}$		0.35 $^{\times2\downarrow\ \times1\rightarrow}$		1.26 $^{\downarrow\rightarrow}$		1.98
O9	0.49 $^{\downarrow\rightarrow}$	0.34 $^{\downarrow\rightarrow}$	0.46 $^{\times2\downarrow\ \times1\rightarrow}$				1.29
Sum	1.99	1.88	1.95	1.98	5.19	4.85	

Note: Bond strength for Zn1 site occupancy of $0.55Zn^{2+}+0.45Cu^{2+}$; P1 site occupancy of $0.64P^{5+}+0.36As^{5+}$. The bond-valence calculations were done using the equation and constants of Brown (1977), $S = \exp[R_0-d_0)/b]$. Bond parameters: Pb^{2+}–O^{2-} from Krivovichev and Brown (2001); Cu^{2+}–O^{2-} Krivovichev (2012); P^{5+}–O^{2-} from Gagné and Hawthorne (2015) and As^{5+}–O^{2-} Brown and Altermatt (1985).

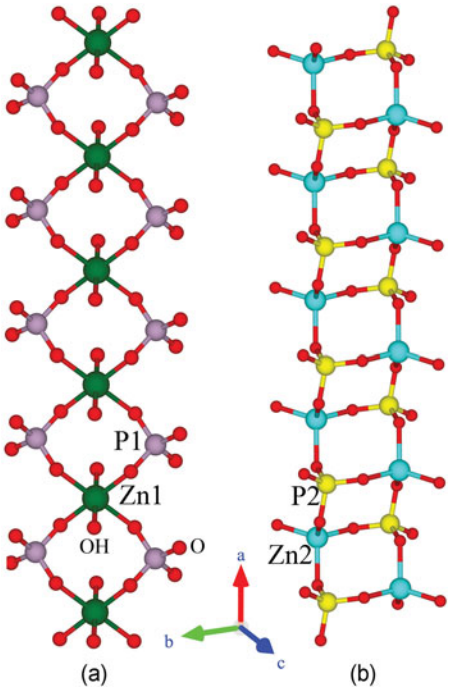

Figure 5. (a) Alternating $ZnO_4(OH)_2$ octahedra and pairs of corner-connected PO_4 tetrahedra forming a tetrahedral–octahedral chain. (b) Double chain of corner-linked ZnO_4 and PO_4 tetrahedra. Each tetrahedron is 3-connected with other tetrahedra in the chain. Key: green= Zn1, blue=Zn2, purple=P1 and yellow = P2.

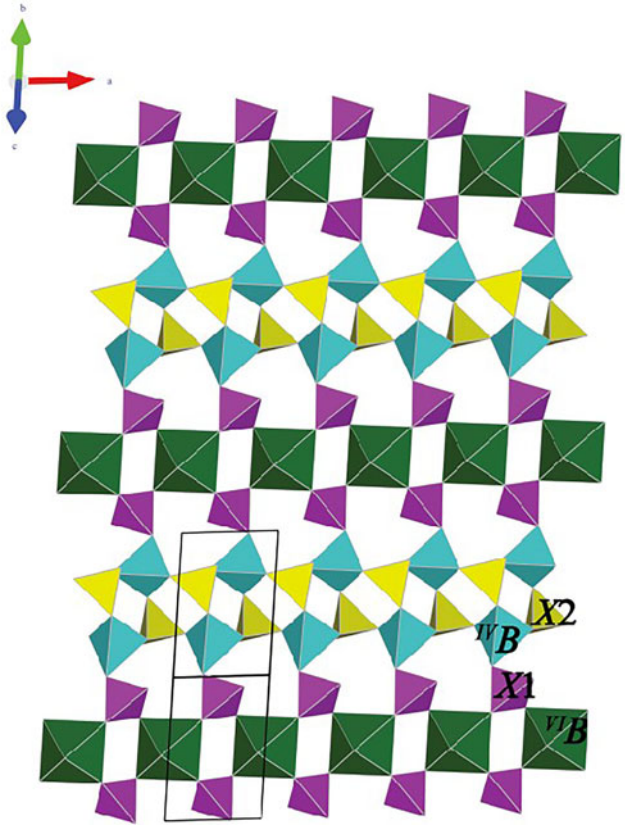

Figure 6. The parallel to (011) layer in dongchuanite; the two types of chains are connected by corner-sharing between $[ZnO_4]$ and $[PO_4]$ tetrahedra forming wrinkled layers parallel to (011). Legend: ^{VI}B: Zn1 octahedra; ^{IV}B: Zn2 tetrahedra; *X*1: P1 tetrahedra; *X*2: P2 tetrahedra.

The Pb^{2+} cations have lone-electron pairs and typically are positioned off-centre in their polyhedral coordination. In dongchuanite (Fig. 7), the stereochemically active $6s^2$ lone-electron-pair of Pb^{2+} results in a 'one-sided' distorted 8-fold coordination, with the Pb–O distance on one side of the ion being longer than on the other. The PbO_8 eight-fold coordination polyhedra are modified square antiprisms with short bonds to four O atoms and much longer bonds to four O atoms. The Pb1–O bond distances have four shorter bonds to anions in the range of 2.32 to 2.61 Å and four longer bonds in the range of 2.91 to 3.05 Å. The Pb2–O has four shorter bonds in the range of 2.36 to 2.53 Å and four longer bonds in the range of 2.96 and 3.42 Å. The shorter bonds are to oxygen ligands of the $P1O_4$ tetrahedra, whilst the longer bonds are to those of the $P2O_4$ tetrahedra. Similar bonding has been reported for Pb in a synthetic lead hydrated phosphate (Mills *et al.*, 2010).

Discussion

On the basis of crystal structure refinement and composition analysis of multiple samples from the mine, we found at least four mineral species with different compositions and similar structure. We propose the use of 'dongchuanite group' to systematically describe such mineral species. We have submitted the proposal to the CNMNC and it is under review. The general crystal chemistry formula of the 'dongchuanite group' minerals exhibit a generalised formula: $A_4{}^{VI}B^{IV}B_2(X1O_4)_2(X2O_4)_2(OH)_2$, where *A* is an interlayer cation with dominant Pb; *B* are transition metals with two

https://doi.org/10.1180/mgm.2023.16 Published online by Cambridge University Press

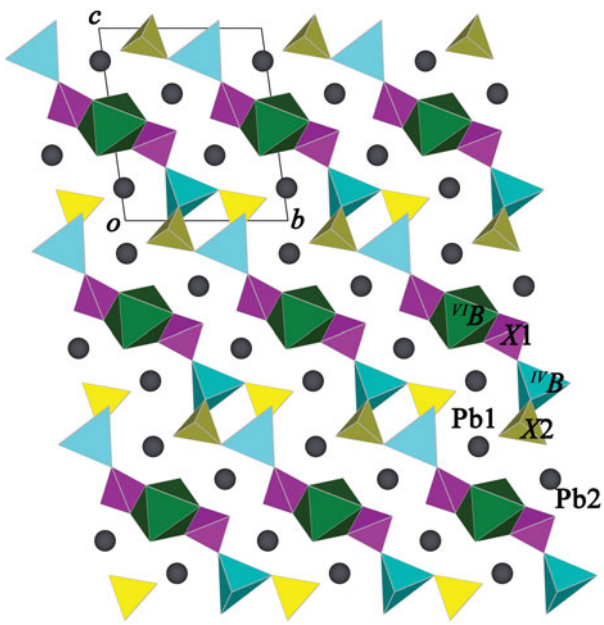

Figure 7. The structure for dongchuanite showing a wrinkled layer. The Pb is located in the wrinkled interlayers. Legend as in Fig. 6.

crystallographic positions; ^{IV}B is in tetrahedral coordination, fully occupied by Zn, whereas ^{VI}B has an octahedral coordination, occupied by Zn, Cu and Fe; and $X1$ and $X2$ are cations in complex anions, which are tetrahedrally coordinated and occupied by P and As.

The distributions of P and As at the $X1$ and $X2$ sites can be calculated from our study of the X-ray crystal structure refinement of the 'dongchuanite group' minerals. As shown in Fig. 8, As-atoms tend to preferentially occupy the $X1$ site. A similar pattern of occupation was also determined in the philipsburgite–kipushite series (Krivovichev *et al.*, 2018). Therefore, to avoid multiple occupancies, As (arsenic) was first assigned to the X1 position, although this may be slightly different from the occupancy of the crystal structure refinement.

The dominant elements in the crystallographic sites are the most important criterion for the definition of a mineral species. In the crystal structure, the $X1$ and $X2$ sites are two different crystallographic locations. $[X1O_4]$ tetrahedra share corners with $[^{IV}BO_4]$ tetrahedra and $[^{VI}BO_4(OH)_2]$ octahedra. $[X2O_4]$ tetrahedra share corners with two $[^{IV}BO_4]$ tetrahedra. X-ray single-structure refinement shows that As occupies the $X1$ site more preferentially than the X2 site. When the atoms per formula unit (apfu) of As is < 0.8, no As atom is observed at the $X2$ site and nearly all As atoms occupy the $X1$ site. When the apfu of As is >1.0, a small amount of As begins to occupy the position $X2$, and the total As at position $X2$ is always lower than that of $X1$. Consistently, the end-members with dominant As at $X2$ and dominant P at $X1$ probably do not exist. Moreover, only when the content of As is high enough (upper right corner area

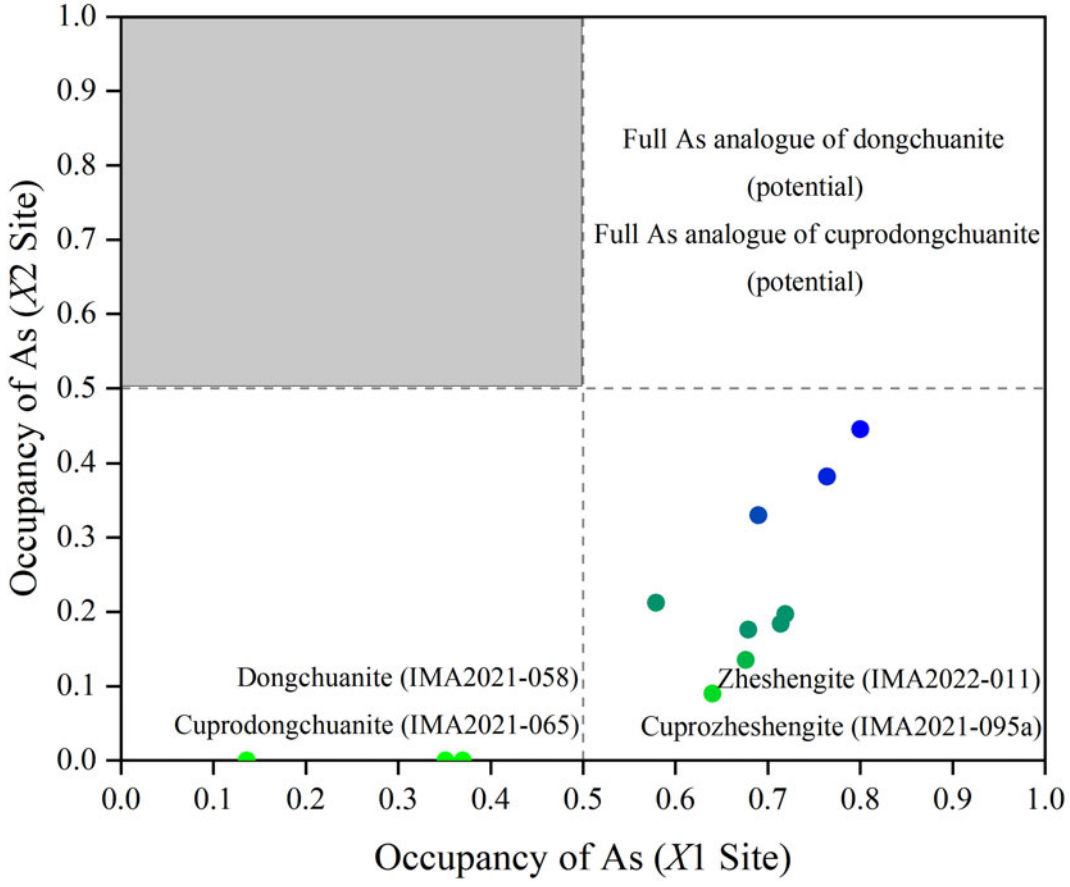

Figure 8. The distribution of As atoms at $X1$ and $X2$ sites based on crystal structure X-ray refinement of 'dongchuanite group' minerals. The results show As atoms tend to occupy the $X1$ position preferentially. The dark grey area is vacant.

https://doi.org/10.1180/mgm.2023.16 Published online by Cambridge University Press

in Fig. 8), can it become dominant at both *X*1 and *X*2 sites, whose end-member formula is $A_4^{VI}B^{IV}B_2(AsO_4)_2(AsO_4)_2(OH)_2$. Therefore, the mineral species of this group can be divided into three ideal end-member formulae. Where P is dominant at both the *X*1 and *X*2 sites gives: $A_4^{VI}B^{IV}B_2(PO_4)_2(PO_4)_2(OH)_2$. The mineral species currently approved by the IMA–CNMNC are dongchuanite, $Pb_4ZnZn_2(PO_4)_2(PO_4)_2(OH)_2$ and cuprodongchuanite, $Pb_4CuZn_2(PO_4)_2(PO_4)_2(OH)_2$. Where As is dominant at the *X*1, and P at the *X*2, the formula is $A_4^{VI}B^{IV}B_2(AsO_4)_2(PO_4)_2(OH)_2$. So far, the approved mineral species are zheshengite, $Pb_4ZnZn_2(AsO_4)_2(PO_4)_2(OH)_2$ and cuprozheshengite, $Pb_4CuZn_2(AsO_4)_2(PO_4)_2(OH)_2$. Where As is dominant at both the *X*1 and *X*2 sites, e.g. $A_4^{VI}B^{IV}B_2(AsO_4)_2(AsO_4)_2(OH)_2$, are potential new minerals.

Summary

Dongchuanite is triclinic. The space group of $P\bar{1}$ exhibits unit-cell parameters: $a = 4.7620(10)$ Å, $b = 8.5070(20)$ Å, $c = 10.3641(19)$ Å, $\alpha = 97.110(17)°$, $\beta = 101.465(17)°$, $\gamma = 92.273(18)°$, $V = 407.44(15)$ Å^3 and $Z = 1$. The crystal structure is a wrinkled layer parallel to (011) formed of corner-sharing tetrahedra and octahedra. The ideal and simplified formulae of dongchuanite are $Pb_4ZnZn_2(PO_4)_2(PO_4)_2(OH)_2$ and $Pb_4(Zn,Cu)Zn_2[(P,As)O_4]_2(PO_4)_2(OH)_2$ respectively.

Dongchuanite is not an isolated mineral species. Instead, it is one species in a new group consisting of many mineral species. The general crystal-chemical formula of the mineral group is $A_4^{VI}B^{IV}B_2(X1O_4)_2(X2O_4)_2(OH)_2$. The structural study demonstrates that the dongchuanite structure type allows for the selective As–P substitution being induced by different crystal chemical environments of two tetrahedral sites, of which the *X*2 site is more preferable for P, whereas the *X*1 site is more suitable for As. The classification and nomenclature of the 'dongchuanite group' will be detailed in a later paper following CNMNC approval.

Supplementary material. The supplementary material for this article can be found at https://doi.org/10.1180/mgm.2023.16.

Acknowledgements. We wish to acknowledge Ritsuro Miyawaki, chairman of the CNMNC, and the Commission members for their valuable suggestions with respect to dongchuanite. We also wish to thank the reviewers for their suggestions and comments. Thanks to Chen Jingwen for taking the SEM photo. This work was supported financially by the National Natural Science Foundation of China (41672043).

Competing interests. The authors declare none.

References

Brown I.D. (1977) Predicting bond lengths in inorganic crystals. *Acta Crystallographica,* **B33**, 1305–1310.

Brown I.D. and Altermatt D. (1985) Bond-valence parameters obtained from a systematic analysis of the inorganic crystal structure database. *Acta Crystallographica,* **B41**, 244–247.

Ciesielczuk J., Janeczek J., Dulski M. and Krzykawski T. (2016) Pseudomalachite–cornwallite and kipushite–philipsburgite solid solutions: chemical composition and Raman spectroscopy. *European Journal of Mineralogy*, **28**, 555–569.

Dolomanov O.V., Bourhis L.J., Gildea R.J., Howard J. and Puschmann H. (2010) Olex2: a complete structure solution, refinement and analysis program. *Journal of Applied Crystallography*, **42**, 339–341.

Farmer C.V. (1974) *The Infrared Spectra of Minerals*. Mineralogical Society Monograph 4, The Mineralogical Society, London, 539 pp.

Frost R.L., Martens W.N. and Williams P.A. (2002) Raman spectroscopy of the phase-related basic copper arsenate minerals olivenite, cornwallite, cornubite and clinoclase. *Journal of Raman Spectroscopy*, **33**, 475–484.

Gagné O.C. and Hawthorne F.C. (2015) Comprehensive derivation of bond-valence parameters for ion pairs involving oxygen. *Acta Crystallographica,* **B71**, 562–578.

Grey I.E., Keck E., Kampf A.R., Macrae C.M., Glenn A.M. and Price J.R. (2017) Wilhelmgümbelite, $[ZnFe^{2+}Fe_3^{3+}(PO_4)_3(OH)_4(H_2O)_5]\cdot 2H_2O$, a new schoonerite-related mineral from the Hagendorfsüd pegmatite, Bavaria. *Mineralogical Magazine*, **81**, 287–296.

Hawthorne F.C., Cooper M.A., Abdu Y.A., Ball N.A., Back M.E. and Tait K.T. (2012) Davidlloydite, ideally $Zn_3(AsO_4)_2(H_2O)_4$, a new arsenate mineral from the Tsumeb mine, Otjikoto (Oshikoto) region, Namibia: description and crystal structure. *Mineralogical Magazine*, **76**, 45–57.

He Y. (1996) Metallogenetic series, deposit type and metallogenetic model of Dongchuan Cu deposit. *Yunnan Geology*, **15**, 320–329.

King G.S.D. and Sengier-Roberts L. (1988) Drugmanite, $Pb_2(Fe_{0.78}Al_{0.22})H(PO_4)_2(OH)_2$: Its crystal structure and place in the datolite group. *Bulletin de Mineralogie*, **111**, 431–437.

Krivovichev S.V. (2012) Derivation of bond-valence parameters for some cation-oxygen pairs on the basis of empirical relationships between r_o and *b*. *Zeitschrift für Kristallographie – Crystalline Materials*, **227**, 575–579.

Krivovichev S.V. and Brown I.D. (2001) Are the compressive effects of encapsulation an artifact of the bond valence parameters? *Zeitschrift für Kristallographie*, **216**, 245–247.

Krivovichev S.V., Zhitova E.S., Ismagilova R.M. and Zolotarev A.A. (2018) Site-selective As–P substitution and hydrogen bonding in the crystal structure of philipsburgite, $Cu_5Zn((As,P)O_4)_2(OH)_6\cdot H_2O$. *Physics and Chemistry of Minerals*, **45**, 917–923.

Leach D.L. and Song Y. (2019) Sediment-hosted zinc-lead and copper deposits in China. Pp. 325–409 in: *Mineral Deposits of China* (Chang, Z. and Goldfarb, R.J., editors). Society of Economic Geologists, Special Publication, **22**. Society of Economic Geologists, Colorado, USA.

Li G., Shen H., Sun N., Xue Y. and Hao J. (2021) Dongchuanite, IMA 2021-058. CNMNC Newsletter 63. *Mineralogical Magazine*, **85**, 910–915, https://doi.org/10.1180/mgm.2021.74

Li G., Sun N., Shen H., Xue Y. and Hao J. (2022) Zheshengite, IMA 2022-011. CNMNC Newsletter 67. *Mineralogical Magazine*, **86**, 849–853, https://doi.org/10.1180/mgm.2022.56

Mandarino J.A. (1981) The Gladstone-Dale relationship: Part IV. The compatibility concept and its application.*The Canadian Mineralogist*, **19**, 441–450.

Mills S.J., Kolitsch U., Miyawaki R., Hatert F., Poirier G., Kampf A.R., Matsubara S. (2010) $Pb_3Fe_2^{3+}(PO_4)_4(H_2O)$, a new octahedral-tetrahedral framework structure with double-strand chains. *European Journal of Mineralogy*, **22**, 595–604.

Sheldrick G.M. (2015) Crystal structure refinement with SHELXL. *Acta Crystallographica*, **C71**, 3–8.

Siegrist T. (1997). Crystallographica – a software toolkit for crystallography. *Journal of Applied Crystallography*, **30**, 418–419.

Sun N., Li G., Xue Y., Shen H. and Hao J. (2021) Cuprodongchuanite, IMA 2021-065. CNMNC Newsletter 63. *Mineralogical Magazine*, **85**, 910–915, https://doi.org/10.1180/mgm.2021.74.

Sun N., Grey I.E., Li G., Rewitzer C., Xue Y., Mumme W.G., Shen H., Hao J., MacRae C.M., Riboldi-Tunnicliffe A., Boer S., Williams T. and Kampf A.R. (2022) Cuprozheshengite, IMA 2021-095a. CNMNC Newsletter 67. *Mineralogical Magazine*, **86**, 849–853, https://doi.org/10.1180/mgm.2022.56.

Zeng R.Y., Jiang H., Zhu X.Y., Zhang X., Xiao J., L X.Q., Hu C., Yang X.K., Li J.L. and Zhen Z.G. (2021) Fluid evolution and mineralization mechanism of Dongchuan copper deposit in Yunnan province. *Geoscience*, **35**, 244–257

Zhang X., Zhu X.Y., Jiang H., Lu X.Q., Wang Y.F., Liu W.J., Tian L.P., Zeng R.Y. and Xiao J. (2021) Metallogenic characteristics and prospecting direction of Dongchuan Copper Deposit, Yunnan Province. *Mineral Exploration*, **12**, 964–971.